Research on Bistatic Sonar Positioning and Its Optimization Algorithm

Hongquan Lei[1], Diquan Li[1], Haidong Jiang[2*]

[1] School of Geosciences and Info-Physics, Central South University, Changsha 410083, China
[2] Institute of Resources and Environmental Engineering, Guizhou Institute of Technology, Guiyang 550003, China

Corresponding Author Email: 20170783@git.edu.cn

ABSTRACT

Since the general bistatic system is a T/R-R type bistatic sonar, both the transmitting and receiving stations can provide measurement data, so there is redundant information. Therefore, the problem of bistatic sonar positioning is essentially the optimization problem of nonlinear systems. In order to make full use of redundant observation information, this paper optimizes the bistatic sonar positioning algorithm. This paper firstly introduces the principle of bistatic sonar positioning, then builds an acoustic emission instrument monitoring system, then introduces the traditional bistatic sonar positioning algorithm, and optimizes the algorithm on the basis of the traditional algorithm, and finally verifies the Optimize the accuracy of the algorithm. Experimental research shows that the optimized algorithm has higher positioning accuracy, and the positioning error is reduced to 0.68 times, which confirms the effectiveness of the research.

1. INTRODUCTION

With the development of submarine stealth technology and underwater acoustic countermeasure technology, higher requirements are put forward for the concealment and anti-interference of sonar equipment [1, 2]. Bistatic sonar, because the transceiver equipment is separated, the system has the working characteristics of active and passive sonar, and can use the existing technology and equipment, so it has great potential advantages in anti-stealth, anti-water acoustic countermeasures, etc. There are two types of bistatic systems: T-R and T/R-R [3, 4]. The general bistatic system is a T/R-R bistatic sonar. Both the transmitting and receiving stations can provide measurement data, so there is redundant information. When solving the positioning performance optimization problem of the T/R-R type bistatic sonar system, it is necessary to consider making full use of the redundant observation information to achieve the purpose of high-precision positioning [5]. The algorithm is optimized.

Many scholars have conducted research on formation fractures. Liu et al. [1] conducted field and experimental studies on ground fissures in the Kenya Rift Valley, and determined the structural characteristics of the underground erosion fissures. Hu et al. [2] introduced various forms of ground fissures, analyzed the formation process of uneven ground subsidence area during the construction of underground engineering, and preliminarily explained the fracture mechanism of soil in the ground fissure area. He et al. [3] investigated the development and formation of ground fissures in the No. 401 panel of Shangwan Coal Mine in Shendong mining area, and clarified the development and formation mechanism of ground fissures. Liu et al. [4] described the origin of collapsible ground fissures by

monitoring the development of collapsible subsidence and the formation of ground fissures. Shi [5] selected typical ground fissure areas as representatives for discussion, and believed that the over-exploitation of groundwater resources and tectonic activities were the main factors causing the formation of ground fissures, and accordingly put forward corresponding prevention suggestions. Although there are many studies on formation fractures, there is still a lack of research on structural fractures in limestone formations.

Sonar is widely used in positioning. Hou et al. [6] discussed the application of side scan sonar and subsea profiler in location of subsea pipeline fractures. Fügenschuh et al. [7] used mixed integer programming to solve the multi-static pressure sonar localization problem, and two natural sensor placement problems were presented. Aiming at the random error problem in multiple sonar positioning systems, Chen and Wang [8] proposed a time-frequency-based Doppler moving target positioning system. Giorli et al. [9] was the first to use dual-frequency identification sonar to characterize fauna in the deep ocean scatter layer and to estimate the numerical density and length of fauna at different depths and locations off the Kona coast of the Big Island of Hawaii. Peters [10] studied the problem of multi-static active sonar positioning targets and developed a more accurate positioning method. Although sonar is widely used for localization, the problem of sonar localization of structural fractures in limestone formations has not been studied.

This paper firstly introduced the principle of sonar positioning, and selected bistatic sonar as the positioning method of limestone fissures, and then constructed an acoustic emission instrument monitoring system. After that, the traditional bistatic sonar algorithm was introduced, and the algorithm was optimized on this basis. In the experimental part,

the influence on the positioning accuracy of the traditional algorithm and the optimization algorithm was studied from four aspects: baseline length, configuration angle, time and orientation error, and site measurement error. The experimental results were used to verify the validity of the research.

2. LIMESTONE FISSURES SONAR POSITIONING SYSTEM

2.1 Principle of sonar positioning

Sonar conducts geological monitoring by emitting sound waves [11]. Acoustic emission localization is to determine the location of the crack source by obtaining the time difference between the acoustic waves at different locations reaching the sensor, and then use the localization algorithm to infer the location of the AE event. The location of the audio emission source is then inferred, and finally the location of the AE event is determined [12].

Multistatic sonar not only has the advantage that active sonar does not depend on target location and known waveform, but also has the advantage of concealing sonar and increasing the working range [13, 14]. Figure 1 shows how a multistatic sonar works.

Figure 1(a) is the distributed-centralized data processing method of multi-static sonar, and Figure 1(b) is the centralized data processing method of multi-static sonar. Distributed-centralized data processing is to divide the multi-base sonar into small units, and upload the positioning results of each small unit to the signal processing center for data fusion processing; centralized data processing is to input the information received by each receiving center directly into the signal processing center.

The smallest unit of multistatic sonar is bistatic sonar [15]. In this paper, dual-base sonar is used to study the location of structural fractures in limestone strata.

2.2 Acoustic emission instrument monitoring system

The acoustic emission instrument monitoring system is shown in Figure 2.

The acoustic emission instrument is a complete integrated data acquisition and processing system, which can track the position of continuous acoustic emission sources in real time. This audio transmitter has 8 channels, the sampling frequency is 10 MHz, its value is set to 100 mV, and the post-amp frequency is 0-20 dB. The acoustic emission system can count the total number of acoustic emission events generated in the entire detection process, and calculate the source data to determine the spatial location of the acoustic emission source.

2.3 Traditional bistatic sonar positioning algorithm

The working principle of bistatic sonar is shown in Figure 3 [16].

In the figure, T/R is the transmitting station, R is the receiving station, and the distance and azimuth from the transmitting station to the target are r_T and θ_r respectively; the distance and azimuth from the receiving station to the target are r_R and θ_R, respectively.
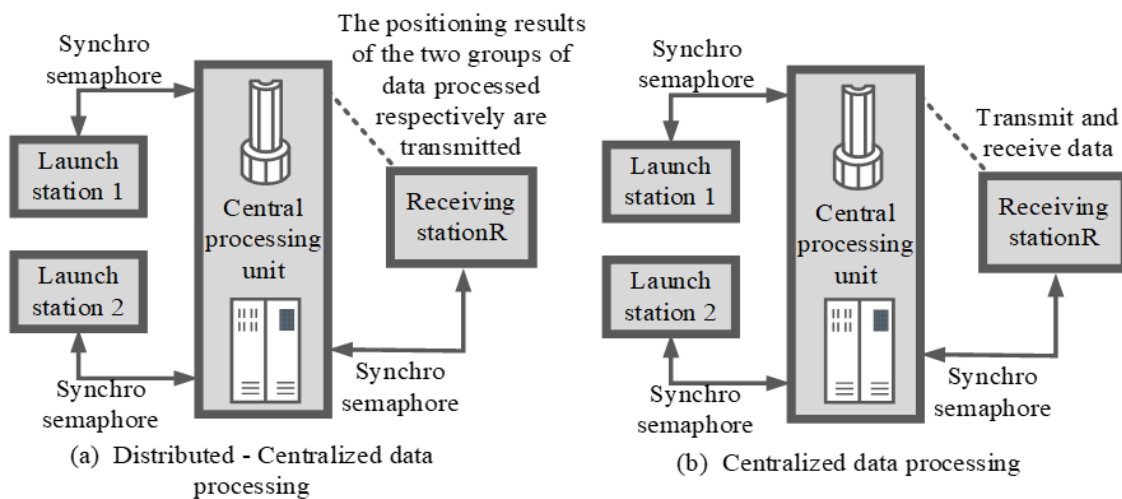

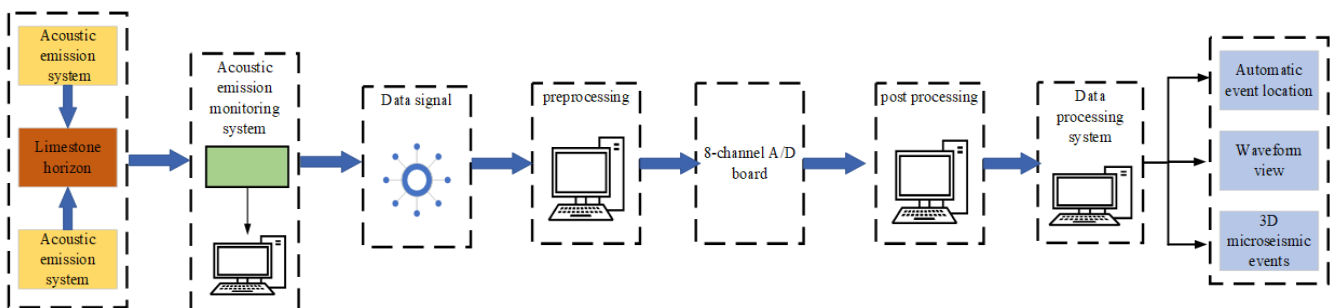**Figure 1.** The way multi-base sonar works

Figure 2. Acoustic emission instrument monitoring system

The traditional bistatic sonar positioning algorithm is based on the time-of-arrival positioning algorithm (TOL algorithm) [17], and its positioning formula is:

$$\rho_R = r_T + \sqrt{(x - x_R)^2 + (y - y_R)^2} \quad (1)$$

$$r_T = \sqrt{(x - x_T)^2 + (y - y_T)^2} \quad (2)$$

$$\rho_R = r_T + r_R \quad (3)$$

By solving this formula, it can be obtained:

$$k_0 = [r_\Sigma^2 + (x_T^2 + y_T^2)^2 - (x_R^2 + y_R^2)^2 - 2r_\Sigma r_T]/2 \quad (4)$$

Then:

$$x = \frac{k_0 - (y_T - y_R)y}{x_T - x_R} \quad (5)$$

Taking this formula into the expression for r_T [18], it can be obtained:

$$ay^2 - 2by + c = 0 \quad (6)$$

Among them:

$$a = (x_T - x_R)^2 + (y_T - y_R)^2 \quad (7)$$

$$b = (k_0 - x_T^2 + x_T x_R)(y_T - y_R) + y_T(x_T - x_R)^2 \quad (8)$$

$$c = (k_0 - x_T^2 + x_T x_R)^2 + (x_T - x_R)^2(y_T^2 - r_T^2) \quad (9)$$

Then:

$$y = \frac{b \pm \sqrt{b^2 - ac}}{a} \quad (10)$$

Since y has a binary solution, there is position uncertainty, so the localization algorithm is invisible in time, and other information such as azimuth must be used to remove the position ambiguity [19]. Substituting the solution of formula (6) into formula (5), two sets of solutions can be obtained, and are respectively brought into the azimuth formula of the launch station to get:

$$\theta_{T1} = arctan \frac{y_1 - y_T}{x_1 - x_T} \quad (11)$$

$$\theta_{T2} = arctan \frac{y_2 - y_T}{x_2 - x_T} \quad (12)$$

Azimuth θ_T is applied to determine:
If $|\theta_{T1} - \theta_T| \leq |\theta_{T2} - \theta_T|$, then $X = [x_1, y_1]^T$. Otherwise, $X = [x_2, y_2]^T$ is taken.
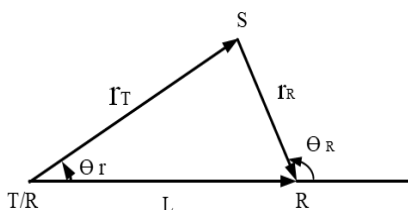

Figure 3. How bistatic radar sonar works

2.4 Bistatic sonar positioning optimization algorithm

Based on the traditional positioning algorithm, this paper proposes a bistatic sonar positioning optimization algorithm (WLS algorithm) based on weighted least squares:

$$\begin{cases} r_T = \sqrt{(x - x_T)^2 + (y - y_T)^2} \\ \theta_T = tan^{-1}[(y - y_T)/(x - x_T)] \end{cases} \quad (13)$$

$$\begin{cases} \rho_R = \sqrt{(x - x_T)^2 + (y - y_T)^2} \\ \quad + \sqrt{(x - x_R)^2 + (y - y_R)^2} \\ \theta_R = tan^{-1}[(y - y_R)/(x - x_R)] \end{cases} \quad (14)$$

By solving the position formulas of the transceiver stations respectively [20], two sets of position solutions can be obtained:

$$X_1 = \begin{bmatrix} x_1 \\ y_1 \end{bmatrix} = \begin{bmatrix} x_T + r_T cos(\theta_T) \\ y_T + r_T sin(\theta_T) \end{bmatrix} \quad (15)$$

$$X_2 = \begin{bmatrix} x_2 \\ y_2 \end{bmatrix} = \begin{bmatrix} x_R + r_R cos(\theta_R) \\ y_R + r_R sin(\theta_R) \end{bmatrix} \quad (16)$$

The two sets of positioning solutions obtained from the transmitter to the receiver station are not exactly the same, so data integration methods can be used to combine them to find the optimal solution [21].

The data measured at the transmitting and receiving stations are:

$$r_T' = r_T + dr_T = (\delta_1 + N(0, \delta_{\tau_1})) \cdot v_c/2 \quad (17)$$

$$\rho_R' = \rho_R + d\rho_R = (\delta_2 + N(0, \delta_{\tau_2})) \cdot v_c \quad (18)$$

$$\theta_R' = \theta_R + d\theta_R \quad (19)$$

$$\theta_T' = \theta_T + d\theta_T \quad (20)$$

δ_1 and δ_2 are the sound wave transit time, and $N(0, \delta_{\tau_1})$ is Gaussian noise with zero mean and δ_{τ_1} variance.

Assuming that each measurement error is Gaussian white noise with zero mean and uncorrelated with each other [22], the corresponding standard deviations are σ_{r_T}, σ_{θ_r}, σ_{θ_R}, and σ_{ρ_R}, respectively, so the weighted least squares estimation of the target and its error covariance matrix are:

$$X_{WLS} = (P_1^{-1} + P_2^{-1})^{-1}(P_1^{-1}X_1 + P_2^{-1}X_2) \quad (21)$$

$$P_{WLS} = (P_1^{-1} + P_2^{-1})^{-1} \quad (22)$$

For the WLS algorithm, the geometrical precision factor (GDOP) is expressed as:

$$GDOP = \sqrt{tr[P_{WLS}]} = \sqrt{\sigma_x^2 + \sigma_y^2} \quad (23)$$

3. EXPERIMENT RESULTS AND DISCUSSION OF SONAR POSITIONING

This paper compares the positioning accuracy of the TOL algorithm and the WLS algorithm, and studies its influence on
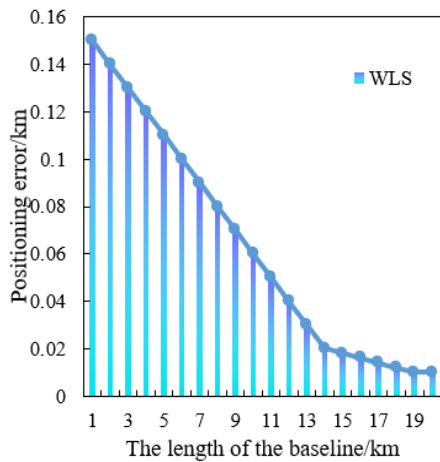
the positioning accuracy of the TOL algorithm and the WLS algorithm from four aspects: baseline length, configuration angle, time and orientation errors, and site measurement errors, and calculates their comprehensive positioning performance.

3.1 Baseline length

Figure 4 shows the effect of baseline length changes on the positioning accuracy of the TOL algorithm and the WLS algorithm.
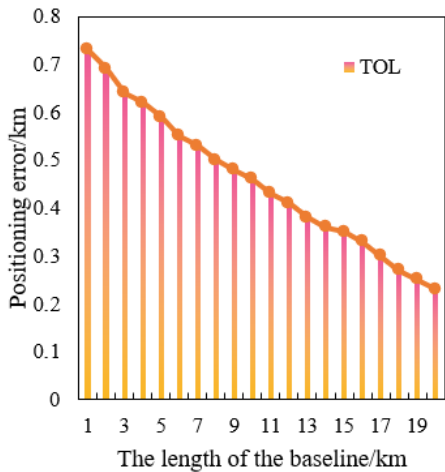
(a) Influence of positioning error on TOL

(b) Influence of positioning error on WLS

Figure 4. Influence of baseline length variation on positioning accuracy

Figure 4(a) shows the effect of the baseline length change on the accuracy of the TOL algorithm, and Figure 4(b) shows the effect of the baseline length change on the accuracy of the WLS algorithm. In Figure 4(a), when the baseline length is 1 km, the positioning error of TOL is 0.73 km, and with the gradual increase of the baseline length, the positioning error of TOL also gradually decreases. When the baseline length is 9 km, the positioning error of TOL is reduced to 0.48 km. When the baseline length is 20 km, the positioning error of TOL is reduced to 0.23 km. It can be seen that the closer to the baseline is, the worse the TOL localization accuracy is. In Fig. 4(b), the variation trend of the positioning error of the WLS algorithm is the same as that of the TOL algorithm. When the baseline length is 1 km, the positioning error of WLS is 0.15 km, and then the positioning error decreases with the increase of the baseline length. When the baseline length is 9 km, the

positioning error of WLS is reduced to 0.07 km. When the baseline length is 14 km, the positioning error of WLS is reduced to 0.02 km. During the process of increasing the baseline length from 14 km to 20 km, the change of the positioning error is relatively slow, and finally decreases to 0.01 km. The comparison data shows that when the baseline length changes, the positioning error of TOL is much higher than that of WLS, and with the increase of positioning error, the accuracy of both TOL and WLS algorithms gradually improves. But compared with the TOL algorithm, the variation of WLS is smaller.
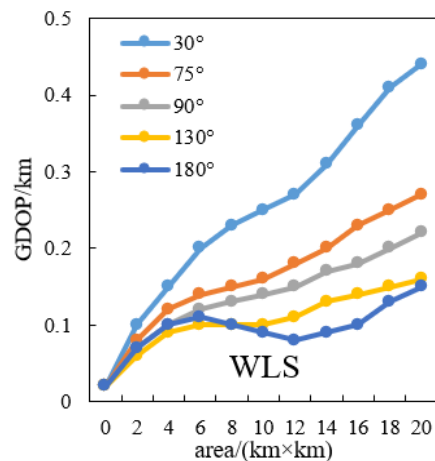
3.2 Configuration angle

The configuration angles of the two sound sources are set as 30º, 75º, 90º, 130º, and 180º in turn. The influence of different sound source configuration angles on the positioning accuracy of the TOL algorithm and the WLS algorithm is shown in Figure 5.

Figure 5(a) shows the effect of the configuration angle change on the accuracy of the TOL algorithm, and Figure 5(b) shows the effect of the configuration angle change on the accuracy of the WLS algorithm.
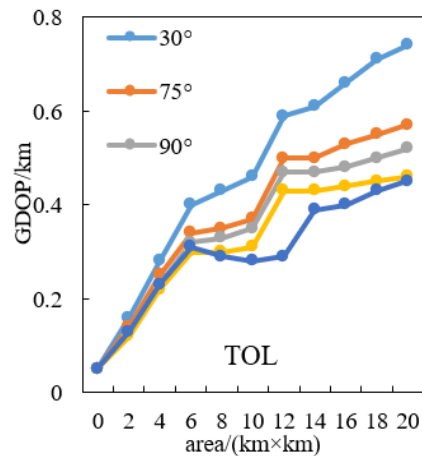
(a) The impact of configuration angles on TOL

(b) The impact of configuration angles on WLS

Figure 5. Influence of different angles of sound source configuration on positioning accuracy

In Figure 5(a), with the gradual increase of the area of the divided area, the GDOP of the TOL algorithm gradually increases, and the localization accuracy of the area gradually deteriorates. When the configuration angle is 30º, the GDOP

is 0.05 km when the area is 0 square kilometers, when the area is 8 square kilometers, the GDOP is increased to 0.43 kilometers, and when the area is 20 square kilometers, the GDOP is raised to 0.74 km. When the configuration angle is 75º, the GDOP is 0.05 km when the area is 0 square kilometers, and when the area is 8 square kilometers, the GDOP is increased to 0.35 km. When the area is 20 square kilometers, the GDOP is increased to 0.57 km. When the configuration angle is 90º, the GDOP is 0.05 km when the area is 0 square kilometers, and when the area is 8 square kilometers, the GDOP is increased to 0.33 km. When the area is 20 square kilometers, the GDOP is increased to 0.52 km. When the configuration angle is 130º, the GDOP is 0.05 km when the area is 0 square kilometers, and when the area is 8 square kilometers, the GDOP is increased to 0.3 km. When the area is 20 square kilometers, the GDOP is increased to 0.46 km. When the configuration angle is 180º, the GDOP is 0.05 km when the area is 0 square kilometers, and when the area is 8 square kilometers, the GDOP is increased to 0.29 km. When the area is 20 square kilometers, the GDOP is increased to 0.45 km. The comparison data shows that when the configuration angle is increased from 30° to 180°, the positioning accuracy of the TOL algorithm gradually decreases, indicating that 180° is the best configuration angle.

In Figure 5(b), the GDOP of the WLS algorithm gradually increases as the area of the divided region gradually increases. When the configuration angle is 30º, the GDOP is 0.05 km when the area is 0 square kilometers, and when the area is 8 square kilometers, the GDOP is increased to 0.23 km. When the area is 20 square kilometers, the GDOP is increased to 0.44 km. When the configuration angle is 75º, the GDOP is 0.05 km when the area is 0 square kilometers, and when the area is 8 square kilometers, the GDOP is increased to 0.15 km. When the area is 20 square kilometers, the GDOP is increased to 0.27 km. When the configuration angle is 90º, the GDOP is 0.05 km when the area is 0 square kilometers, and when the area is 8 square kilometers, the GDOP is increased to 0.13 km. When the area is 20 square kilometers, the GDOP is increased to 0.22 km. When the configuration angle is 130º, the GDOP is 0.05 km when the area is 0 square kilometers, and when the area is 8 square kilometers, the GDOP is increased to 0.1 km. When the area is 20 square kilometers, the GDOP is increased to 0.16 km. When the configuration angle is 180º, the GDOP is 0.05 km when the area is 0 square kilometers, and when the area is 8 square kilometers, the GDOP is increased to 0.1 km. When the area is 20 square kilometers, the GDOP is raised to 0.15 km. The comparison data shows that when the configuration angle is increased from 30° to 180°, the positioning accuracy of the WLS algorithm gradually decreases, indicating that 180° is the best configuration angle.

Comparing the data in the figure, with the change of the configuration angle, the change of the positioning accuracy of the TOL algorithm is the same as the change of the positioning accuracy of the WLS algorithm. However, the GDOP of the TOL algorithm is much higher than that of the WLS algorithm, indicating that the WLS algorithm has higher positioning accuracy.

3.3 Time and orientation errors

The time measurement error is set to δ=30ms, 50ms, the azimuth measurement error is set to σ=0.3°, 1.0°, and the configuration angle is 90°. The influence of different time and azimuth measurement errors on the positioning accuracy of the
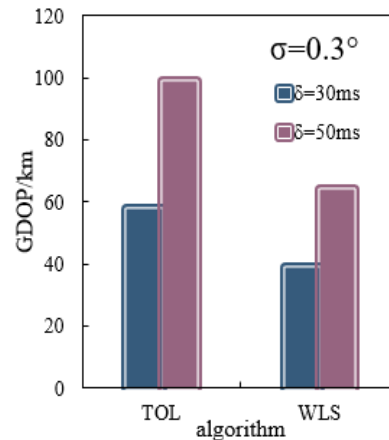
TOL algorithm and the WLS algorithm is shown in Table 1 and Figure 6.

Table 1. Influence of different time and azimuth measurement errors on positioning accuracy

Algorithm			TOL	WLS
GDOP/m	δ=30ms	σ=0.3°	58	39
	δ=30ms	σ=1.0°	56	40
	δ=50ms	σ=0.3°	99	64
	δ=50ms	σ=1.0°	91	66
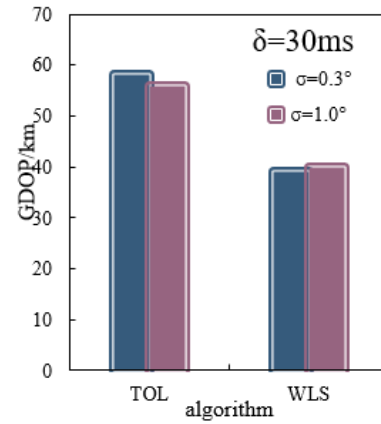
(a) The influence of azimuth error on the algorithm

(b) The influence of time error on the algorithm

Figure 6. Influence of different time and azimuth measurement errors on positioning accuracy
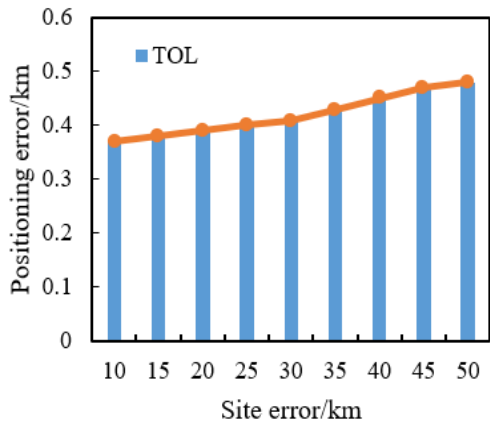
Figure 6(a) shows the influence of the azimuth measurement error on the accuracy of the TOL algorithm when δ=30ms, and Figure 6(b) shows the influence of the time measurement error on the accuracy of the WLS algorithm when σ=0.3°. In Figure 6(a), when σ=0.3°, the GDOP of the TOL algorithm is 58 meters, and the GDOP of the WLS algorithm is 39 meters. When σ=1.0°, the GDOP of the TOL algorithm is 56 meters, and the GDOP of the WLS algorithm is 40 meters. In Figure 6(b), when δ=30ms, the GDOP of the TOL algorithm is 58 meters, and the GDOP of the WLS algorithm is 39 meters. When δ=50ms, the GDOP of the TOL algorithm is 99 meters, and the GDOP of the WLS algorithm is 64 meters. It can be seen from the data that the time measurement error has a great influence on the positioning accuracy of the TOL algorithm and the WLS algorithm. When the time measurement error increases, the GDOP of the two algorithms is greatly improved, that is, the positioning

accuracy of the algorithm decreases. Comparing the data of the two algorithms, it can be seen that the GDOP of the TOL algorithm is higher, indicating that the WLS algorithm is more accurate in positioning.

3.4 Site measurement error

The site measurement error is set to 10m, 20m, and 50m. The influence of the site measurement error on the positioning accuracy of the TOL algorithm and the WLS algorithm is shown in Figure 7.

(a) Influence of site error on TOL
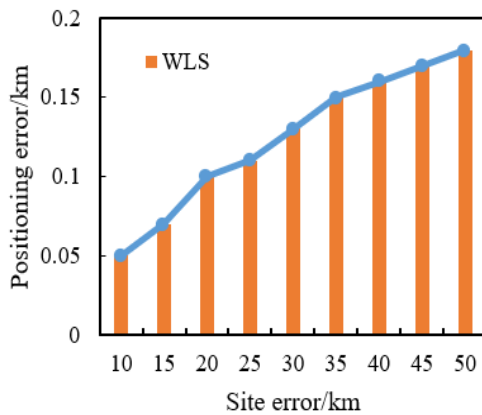
(b) Influence of site error on WLS

Figure 7. Influence of site error on location accuracy

Figure 7(a) shows the influence of the site measurement error on the accuracy of the TOL algorithm, and Figure 7(b) shows the influence of the site measurement error on the accuracy of the WLS algorithm. In Figure 7(a), when the site measurement error is 10 km, the TOL positioning error is 0.37 km. As the site measurement error gradually increases, the TOL positioning error also gradually increases. When the site measurement error is 30 kilometers, the positioning error of TOL increases to 0.41 kilometers. When the site measurement error is 50 kilometers, the positioning error of TOL increases to 0.48 kilometers. It can be seen that the larger the site measurement error is, the worse the TOL positioning accuracy is. In Figure 7(b), the variation trend of the positioning error of the WLS algorithm is the same as that of the TOL algorithm. When the site measurement error is 10 km, the WLS positioning error is 0.05 km, and then the positioning error increases with the increase of the site measurement error. When the site measurement error is 30 kilometers, the WLS positioning error increases to 0.13 kilometers. When the site

measurement error is 50 kilometers, the WLS positioning error increases to 0.18 kilometers. Comparing the data, it can be seen that when the site measurement error changes, the positioning error of TOL is much higher than that of WLS, indicating that the WLS algorithm has higher positioning accuracy.

3.5 Comprehensive positioning performance

The average localization performance of the detection area is expressed as:

$$\overline{GDOP} = \frac{\sum_{i=1}^{N} GDOP(x_i, y_i)}{N} \qquad (24)$$

In the formula, N represents the number of detection sample points in a given area; $\overline{GDOP}$ represents the average GDOP of all detection points in the detection area. With a sufficient number of samples, the comprehensive localization performance of a given area can be approximately characterized. By summarizing the positioning data of the TOL algorithm and the positioning data of the WLS algorithm, the comprehensive positioning performance can be obtained. It is calculated that the $\overline{GDOP}$ of the TOL algorithm is 84 meters, the $\overline{GDOP}$ of the WLS algorithm is 57 meters, and the positioning error of the improved algorithm is reduced to 0.68 times of the original.

4. CONCLUSIONS

In this paper, the bistatic sonar positioning method is used for positioning research, an acoustic emission instrument monitoring system is constructed, and the algorithm is optimized on the basis of the traditional bistatic sonar positioning algorithm. In the experiment part, experiments are carried out on the traditional algorithm and the optimization algorithm from four aspects: Baseline length, configuration angle, time and orientation error, and site measurement error. With lower localization error, the average localization performance of the detection area is better, indicating that the research is feasible.

REFERENCES

[1] Liu, Y., Peng, J.B., Jiang, F.Q., Lu, Q.Z., Zhu, F.J., Qiang, X. (2022). Model test study on the formation and development of underground erosion ground fissures in

the Kenya Rift Valley. Journal of Mountain Science, 19(4): 1037-1050. https://doi.org/10.1007/s11629-021-7004-z

[2] Hu, T., Zhang, J., Li, Q., Wang, W., Liu, J. (2021). Study on formation mechanism of ground fissures induced by underground engineering construction in Chongqing area. In IOP Conference Series: Earth and Environmental Science, 687(1): 15-17. https://doi.org/10.1088/1755-1315/687/1/012045

[3] He, X., Zhao, Y., Yang, K., Zhang, C., Han, P. (2021). Development and formation of ground fissures induced by an ultra large mining height longwall panel in Shendong mining area. Bulletin of Engineering Geology and the Environment, 80: 7879-7898. https://doi.org/10.1007/s10064-021-02429-6

[4] Liu, Z., Lu, Q., Qiao, J., Fan, W. (2021). In situ water immersion research on the formation mechanism of collapsible earth fissures. Engineering Geology, 280(1): 105936-105938.
https://doi.org/10.1016/j.enggeo.2020.105936

[5] Shi, K. W. (2019). Study on formation mechanism of mixed genetic ground fissures in Beijing plain. Journal of Hebei GEO University, 34(8): 173-182.

[6] Hou, Z., Shi, J., Bin, H.U. (2017). Application of side-scan sonar and sub-bottom profiler in locating fracture positions of submarine pipelines. Hydrographic Surveying and Charting, 37(1): 79-82.

[7] Fügenschuh, A.R., Craparo, E.M., Karatas, M., Buttrey, S.E. (2020). Solving multistatic sonar location problems with mixed-integer programming. Optimization and Engineering, 21: 273-303. https://doi.org/10.1007/s11081-019-09445-2

[8] Chen, W.W., Wang, X. (2018). A moving object localization algorithm in a multi-static sonar system with sensor location errors. Computer Engineering & Science, 40(3): 456-463.

[9] Giorli, G., Drazen, J.C., Neuheimer, A.B., Copeland, A., Au, W.W. (2018). Deep sea animal density and size estimated using a Dual-frequency IDentification SONar (DIDSON) offshore the island of Hawaii. Progress in Oceanography, 160(2): 155-166. https://doi.org/10.1016/j.pocean.2018.01.002

[10] Peters, D.J. (2016). A Bayesian method for localization by multistatic active sonar. IEEE Journal of Oceanic Engineering, 42(1): 135-142. https://doi.org/10.1109/JOE.2016.2540744

[11] Krasheninnikov, V.R., Kuvaiskova, Y. E., Malenova, O. E., Subbotin, A.Y. (2021). Testing Hypotheses about Covariance Functions of Cylindrical and Circular Images. Pattern Recognition and Image Analysis, 31: 431-442. https://doi.org/10.1134/S1054661821030159

[12] Zhang, L.M., Cong, Y., Meng, F.Z., Wang, Z.Q., Zhang, P., Gao, S. (2021). Energy evolution analysis and failure criteria for rock under different stress paths. Acta Geotechnica, 16(2): 569-580. https://doi.org/10.1007/s11440-020-01028-1

[13] Ampilov, Y.P., Terekhina, Y.E., Tokarev, M.Y. (2019). Applied aspects of different frequency bands of seismic and water acoustic investigations on the shelf. Izvestiya, Atmospheric and Oceanic Physics, 55: 705-720. https://doi.org/10.1134/S0001433819070028

[14] Zhang, L.M., Wang, X.S., Cong, Y., Wang, Z.Q., Liu, J. (2023). Transfer mechanism and criteria for static–dynamic failure of granite under true triaxial unloading test. Geomechanics and Geophysics for Geo-Energy and Geo-Resources, 9: 104. https://doi.org/10.1007/s40948-023-00645-w

[15] Wei, M., Bian, H., Li, S., Zhang, F. (2021). Mutual information re-registration of sensitive region in forward-looking sonar images combined with particle swarm optimization algorithm. IEEE Access, 9: 7064-7075. 10.1109/ACCESS.2021.3049521

[16] Xiong, J., Wang, W.Q., Cui, C., Gao, K. (2017). Cognitive FDA-MIMO radar for LPI transmit beamforming. IET Radar, Sonar & Navigation, 11(10): 1574-1580. https://doi.org/10.1049/iet-rsn.2016.0551

[17] Li, S., Liu, N., Zhang, L., Zhang, J., Tang, S., Huang, X. (2018). Transmit beampattern synthesis for MIMO radar using extended circulating code. IET Radar, Sonar & Navigation, 12(6): 610-616. https://doi.org/10.1049/iet-rsn.2017.0386

[18] Wu, K.J., Gregory, T. S., Moore, J., Hooper, B., Lewis, D., Tse, Z.T.H. (2017). Development of an indoor guidance system for unmanned aerial vehicles with power industry applications. IET Radar, Sonar & Navigation, 11(1): 212-218. https://doi.org/10.1049/iet-rsn.2016.0232

[19] Wang, C., Li, Z., Zhang, X. (2020). FDA-MIMO for joint angle and range estimation: Unfolded coprime framework and parameter estimation algorithm. IET Radar, Sonar & Navigation, 14(6): 917-926. https://doi.org/10.1049/iet-rsn.2019.0479

[20] Negahdaripour, S. (2018). Application of forward-scan sonar stereo for 3-D scene reconstruction. IEEE Journal of Oceanic Engineering, 45(2): 547-562. https://doi.org/10.1109/JOE.2018.2875574

[21] Peng, D., Zhou, T., Folkesson, J., Xu, C. (2019). Robust particle filter based on Huber function for underwater terrain-aided navigation. IET Radar, Sonar & Navigation, 13(11): 1867-1875. https://doi.org/10.1049/iet-rsn.2019.0123

[22] Liu, W., Yuan, H., Ge, J. (2019). Local-area nanosecond-accuracy time synchronisation based on GPS L1 observations. IET Radar, Sonar & Navigation, 13(5): 824-829. https://doi.org/10.1049/iet-rsn.2018.5283